Unraveling the mechanisms responsible for the interfacial region formation in 4H-SiC dry thermal oxidation

G. H. S. Dartora, E. Pitthan, and F. C. Stedile

Citation: Journal of Applied Physics **122**, 215301 (2017); doi: 10.1063/1.4999332
View online: https://doi.org/10.1063/1.4999332
View Table of Contents: http://aip.scitation.org/toc/jap/122/21
Published by the American Institute of Physics

Articles you may be interested in

Determination of stress components in 4H-SiC power devices via Raman spectroscopy
Journal of Applied Physics **122**, 195703 (2017); 10.1063/1.5003613

Cubic crystalline erbium oxide growth on GaN(0001) by atomic layer deposition
Journal of Applied Physics **122**, 215302 (2017); 10.1063/1.4999342

Local structural determination of N at SiO_2/SiC $(000\bar{1})$ interfaces by photoelectron diffraction
Applied Physics Letters **111**, 201603 (2017); 10.1063/1.4997080

Disorder induced gap states as a cause of threshold voltage instabilities in Al_2O_3/AlGaN/GaN metal-oxide-semiconductor high-electron-mobility transistors
Journal of Applied Physics **122**, 224504 (2017); 10.1063/1.5000497

Single photon sources in 4H-SiC metal-oxide-semiconductor field-effect transistors
Applied Physics Letters **112**, 031105 (2018); 10.1063/1.4994241

Self-trapped holes in β-Ga_2O_3 crystals
Journal of Applied Physics **122**, 215703 (2017); 10.1063/1.5007095

AIP | Journal of Applied Physics SPECIAL TOPICS

JOURNAL OF APPLIED PHYSICS **122**, 215301 (2017)

Unraveling the mechanisms responsible for the interfacial region formation in 4H-SiC dry thermal oxidation

G. H. S. Dartora,[1,a)] E. Pitthan,[2] and F. C. Stedile[1,3]
[1]*PGMICRO, Universidade Federal do Rio Grande do Sul, 91509-900 Porto Alegre, RS, Brazil*
[2]*Instituto de Física, Universidade Federal do Rio Grande do Sul, 91509-900 Porto Alegre, RS, Brazil*
[3]*Instituto de Química, Universidade Federal do Rio Grande do Sul, 91509-900 Porto Alegre, RS, Brazil*

(Received 7 August 2017; accepted 7 November 2017; published online 1 December 2017)

Aiming to understand the processes involved in the formation of the transition region between SiO_2 and SiC, known as the interfacial region, early steps of SiC oxidation were investigated using mainly nuclear reaction analyses. Oxidation kinetics reveals that an abrupt change in the oxidation mechanism is observed in C-face oxide films when their thickness is around 10 nm, while a continuous change in the oxidation mechanism is observed in Si-face oxide films with thicknesses up to about 4 nm. This last thickness corresponds to the maximum width of the interfacial region. Changes observed in the oxidation mechanism were related to oxidation reaction and interfacial atom emission that may take place during oxide film growth. Besides, the activation energies of such processes were obtained. *Published by AIP Publishing.* https://doi.org/10.1063/1.4999332

I. INTRODUCTION

Silicon (Si) still is the most used semiconductor in the micro- and nanoelectronics industry. The possibility to grow an oxide film with great interface properties allowed the conception of several silicon metal-oxide semiconductor (MOS) devices. However, Si physical properties are insufficient for applications that involve high voltage, temperature, power, and frequency. For such applications, silicon carbide (SiC) is a good alternative,[1] since it is a wide bandgap material (3.2 eV for 4H-SiC), with high breakdown field (2.8 MV cm^{-1}), thermal conductivity (4.9 W $cm^{-1}K^{-1}$, higher than that of copper), and saturation velocity (2×10^7 cm s^{-1}).[1] In addition, SiC is the only semiconductor, besides Si, on which a silicon dioxide (SiO_2) film can be thermally grown, allowing us to adapt a good part of Si MOS technology to SiC. However, it presents slower oxidation rates than Si[1] and a channel mobility much lower than the value expected from the bulk material.[1] This fact is mainly attributed to the presence of a high density of electrically active defects in the SiC/SiO_2 interfacial region, which is not as abrupt as in the case of Si,[2,3] and where incompletely oxidized Si and C can be found, mainly in the form of silicon oxycarbides.[4–6] Since it is believed that channel mobility is closely related to the quality of the SiC/SiO_2 interfacial region, a better understanding of the mechanisms taking place in early steps of SiC thermal oxidation, which is when the interfacial region is being formed, is crucial for the improvement of SiC-MOSFET devices.

Some years ago, Hijikata *et al.* proposed a kinetic model based on interfacial Si and C emission.[7] Later on, both Si and C emission from the substrate could be verified.[8,9] Recently, Goto and Hijikata proposed an unified theory for SiC dry thermal oxidation,[10] based on the interfacial Si and C emission model, which manages to describe oxide growth in the entire oxide thickness range. In the present work, we have found that different processes take place during the interfacial region formation and that some of them can be related to atom emission from the substrate, corroborating Goto and Hijikata hypothesis. Moreover, we obtained activation energies (E_a) of those processes for thermal oxidations carried out in conditions known to yield good interfacial properties, such as low oxygen pressure.[4]

II. EXPERIMENTAL PROCEDURES

Samples cut $5 \times 5\,mm^2$ from a 3-in. single crystalline 4H-SiC, non-epitaxial, on-axis, nitrogen doped with N_D-N_A $= 3.1 \times 10^{15}\,cm^{-3}$, research grade wafer, polished on both C $(000\bar{1})$ and Si (0001) faces, purchased from CREE Inc. were employed as substrates. In order to achieve surface cleanliness and uniformity among samples, they were chemically treated following the same procedure:[11] piranha solution (H_2SO_4 95% and H_2O_2, 4:1), standard RCA process,[12] and HF etching (H_2O and HF 40%, 9:1). Each step lasted 10 min at 80 °C, except the HF etching that lasted 1 min at room temperature. After each solution, samples were rinsed with deionized water. As soon as the cleaning steps were over, samples were dried with gaseous nitrogen (N_2) and immediately loaded into the static-atmosphere quartz-tube reactor, where vacuum pumping took place, reaching 10^{-8} mbar. By using a liquid nitrogen trap, oxidations were performed in a dry atmosphere (<1 ppm H_2O). The oxidant species was oxygen enriched at 97% in the ^{18}O isotope, named $^{18}O_2$. The use of ^{18}O allows high selectivity due to its scarce natural abundance (natural oxygen is composed of 99.8% of ^{16}O and 0.2% of ^{18}O). With the $^{18}O(p,\alpha)^{15}N$ nuclear reaction, exclusive to the ^{18}O nuclide, it is possible to differentiate between oxygen incorporation sources other than the thermal treatment, such as from air exposure. In addition, all samples were oxidized using a "u-shaped" sample holder, such that both C and Si faces were exposed to $^{18}O_2$ and oxidized simultaneously. The idea was to grow thin thermal oxide

a)E-mail: gustavo.dartora@ufrgs.br

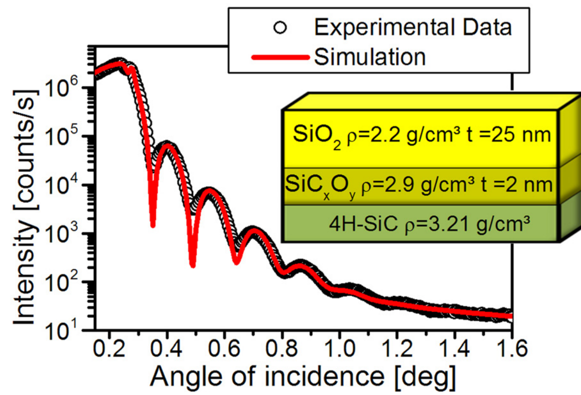

FIG. 1. X-ray reflectivity (XRR) data of the C-face oxide film from the sample oxidized for 60 min in 200 mbar of $^{18}O_2$ at 1150 °C. Black points represent experimental data and the red solid curve represents simulated data. The inset includes parameters (layer composition, density, and thickness) used for simulating experimental data.

films in such a way that the interfacial region is still under formation, allowing us to study the effects of the parameters involved, namely, temperature, pressure, and duration of the thermal treatment. For that, low oxidation rates with different combinations of parameters were used. Thermal treatments were carried out in different combinations of $^{18}O_2$ pressure (100, 150, and 200 mbar), temperature (900, 1000, 1100, and 1150 °C), and time (∼4, 30, 45, 60, and 150 min). The notation "∼4 min" represents the time needed for the sample to go from room temperature to oxidation temperature, which is 3 min for 900 °C and 4.5 min for 1150 °C. Analyses consist of measuring the depth distribution of ^{18}O by Nuclear Reaction Profiling (NRP), simulating experimental data using the FLATUS code,[13] as well as determining the total amount (also known as areal density) of ^{18}O incorporated in each sample by Nuclear Reaction Analysis (NRA),[14] by correlating the sample signal with the signal of a standard $Si^{18}O_2$ film on Si.[15] Both information were achieved using the nuclear reaction on ^{18}O mentioned above, with proton beams about 151 and at 730 keV, to induce NRP and NRA, respectively. Assuming that films are stoichiometric with a given SiO_2 density, the oxide thickness can be determined from NRA results. In this work, we used 2.2 g/cm^{-3} as SiO_2 density, as determined from an X-ray reflectivity measurement (Fig. 1). Note that this is roughly the same density for SiO_2 films thermally grown on Si.[16] Although this conversion is an approximation, since the density of SiO_2 films grown on SiC is shown to be non-uniform (see Fig. 1 and Ref. 17), the ^{18}O areal density data remain valid because they are directly related to oxygen incorporation. Thus, in all plots, besides ^{18}O areal density, the "oxide thickness" will be also included for the sake of comparison with results obtained using other analytical techniques.

III. RESULTS AND DISCUSSION

In the case of present samples, oxygen incorporation ranged from 3.7×10^{15} to 1.2×10^{17} atoms/cm^2, yielding oxide film thicknesses between ∼1 and ∼27 nm. In Fig. 2 are the experimental data for both SiC polar faces of all sets of samples. All experimental points were fitted by straight lines, evidencing that the growth is not diffusion-limited[18] for both faces in the thickness range investigated. Oxygen incorporation rates (α) extracted as the slopes of Fig. 2 fittings were used to generate Arrhenius plots for C-face and Si-face oxide films, which will be shown through the text.

Since extensive work regarding analysis of the physical and compositional properties of the transition layer between SiC and SiO_2 has already been done,[4,6,19–21] revealing, among other facts, that this interfacial region is composed of silicon oxycarbides, we will focus on relating those properties to oxidation kinetics, mechanisms, and models available in the literature. Figure 1 shows that interfacial region density is in between those of SiC and SiO_2, being in accordance

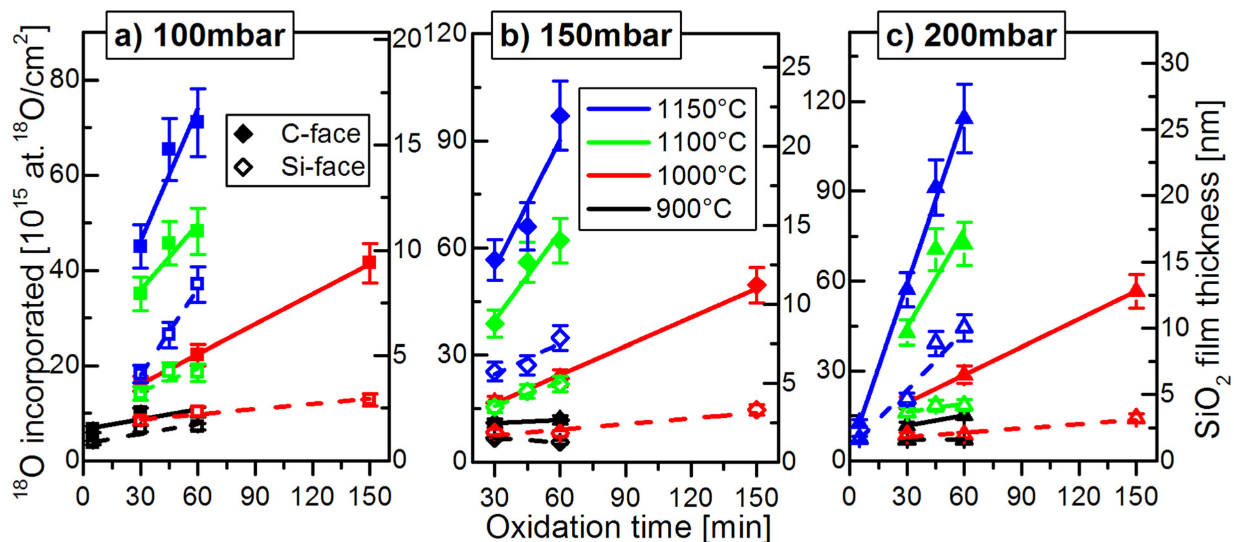

FIG. 2. Time dependence of ^{18}O incorporation for oxidations performed under (a) 100 mbar (squares), (b) 150 mbar (diamonds), and (c) 200 mbar (triangles) of $^{18}O_2$ at different temperatures depicted in (b). Points represent experimental data and lines represent fittings. Full symbols and solid lines concern (000$\bar{1}$) C-face oxidations while empty symbols and dashed lines concern (0001) Si-face oxidation. All plots share the same symbol key and axes units. In the right-hand Y axes are film thicknesses that were determined assuming a uniform SiO_2 film density equal to 2.2 g/cm^3. Bars represent an overall experimental inaccuracy of 10%.

TABLE I. Comparison between parameters of X-ray reflectivity (XRR) measurements performed in this investigation (see Fig. 1) and those of Ref. 22. Note that both studies are in good agreement, revealing that the interfacial region has an intermediate density value when compared to densities of SiC and of SiO_2.

	Density (g/cm^3)			Thickness (nm)	
Sample	4H-SiC	Interfacial region	SiO_2 film	Interfacial region	SiO_2 film
This investigation	3.21	2.9	2.2	2	25
Ref. 22	3.21	2.8	2.3	2	26

with previous findings,[22] as shown in Table I. Moreover, NRP data and simulations shown in Fig. 3 reveal that the Si-face interfacial region presents a gradual oxygen concentration profile and reaches a maximum width of ~4 nm (measured from 90% to 10% of maximum ^{18}O concentration, which is presented as SiO_2 stoichiometry in the inset of Fig. 3) irrespective of total oxide thickness. A similar behavior was observed for C-face oxide films (not shown) and is in accordance with previous findings.[23] According to the "Si and C emission model,"[7,10] SiC oxidation is facilitated by the strain generated due to the expansion of the SiC lattice in order to form amorphous SiO_2, which has a lower atomic density than SiC. As the oxide film thickens up, interstitials accumulate and reduce the oxidation rate, which is interpreted as the oxygen incorporation rate in this work. If this is true, atom emission from the substrate should be intrinsically related to the formation of the interfacial oxycarbide region. Based on the results from Figs. 1 and 3, we suggest that atom emission processes may be the cause for the gradual oxygen concentration profile observed, and the reduction in the emission process may be a result of an ease in the strain, caused by a variation in the density of the interfacial region, which tends to smooth the density gradient from that of SiC to the one of SiO_2 as the interstitials accumulate and get oxidized. Our hypothesis is in accordance with the very recent work concerning the strained interfacial region by Li *et al.*,[24] which reveals that the stress in the oxide film is higher in the initial stages of oxidation and is reduced as the oxide thickens up.

Figure 4 presents oxygen incorporation as a function of oxidation temperature for Si-face oxide films. A non-linear

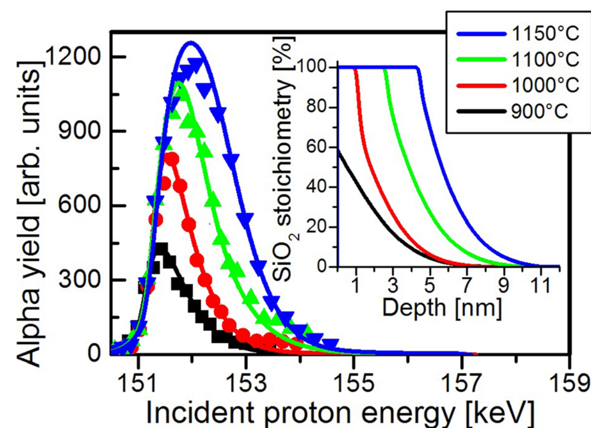

FIG. 3. Nuclear reaction profiling (NRP) analysis for Si-face oxide films grown for 1 h under 100 mbar of $^{18}O_2$ at indicated temperatures. Points represent experimental data and lines represent simulated data. In the inset are ^{18}O concentration profiles used for simulating experimental data using the same scheme of colors. Note that the interfacial region has roughly the same thickness (~4 nm between 90% and 10% of maximum concentration) for all oxide films.

relationship was observed in the logarithmic-linear plot, indicating that oxide thickness dependence on temperature is not exponential. Note that an exponential relationship with temperature would be expected for a process activated only by temperature, as given by the Arrhenius equation. Thus, a mechanism other than thermal activation, such as atom emission due to strain, which does not depend on temperature, should be taking part in the early steps of SiC oxidation. The figure also reveals that Si-face oxide films incorporated similar amounts of ^{18}O (about 7×10^{15} O/cm^2 corresponding to a ~2 nm stoichiometric SiO_2 film) when oxidations were carried out at 900 and 1000 °C, irrespective of $^{18}O_2$ pressure and oxidation time. Remember that, as evidenced in Fig. 3, the oxide film is not stoichiometric in this stage of oxidation, consisting of a layer of silicon oxicarbides. Nevertheless, this indicates a huge reduction in the oxidation rate as compared to the very early oxidation steps, since samples oxidized at 900 and 1000 °C for 60 min presented roughly the same ^{18}O incorporation as samples oxidized for 30 min. Moreover, it suggests that those layers were formed very rapidly, before 30 min of oxidation. Such very rapid growth was also observed on other investigations.[25] This very rapid

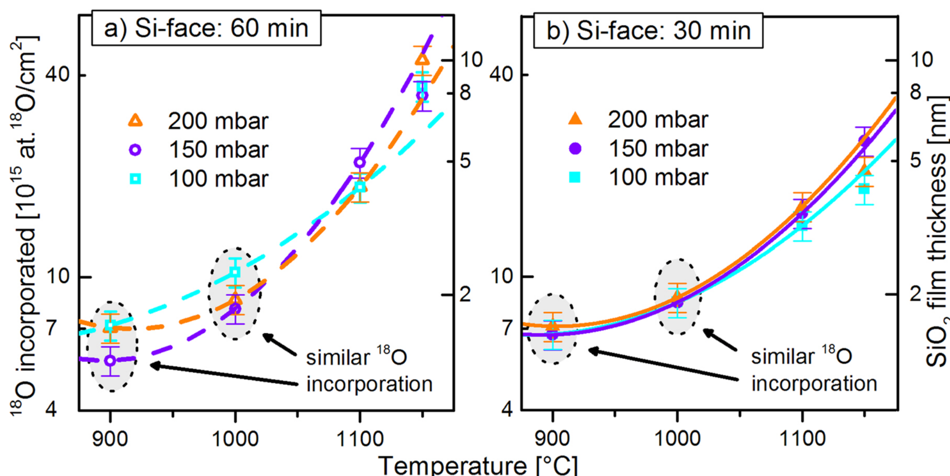

FIG. 4. Temperature dependence of ^{18}O incorporation for Si-face oxide films. Points represent experimental data and lines represent fitting curves related to (a) 60 min samples and (b) 30 min samples. Fitting curves are only to guide the eyes. Ellipses indicate the situation in which similar amounts of oxygen were incorporated when oxidations were carried out at 900 and 1000 °C, irrespective of $^{18}O_2$ pressure or oxidation time. Bars represent an overall experimental inaccuracy of 10%.

growth followed by a reduction in the oxidation rate can also be observed in the Arrhenius plots for oxidation rates in Si-face films (Fig. 5), where it is shown that the oxide growth rate determined for Si-face oxide films grown at 900 °C and 100 mbar is about 0.016 nm/min, (which is as fast as the C-face oxide growth rate under the same conditions), and this growth rate is reduced to 0.008 nm/min as the oxide film reaches the thicknesses used to calculate growth rates presented for oxides grown at 1000 °C and 100 mbar. This evidences that the oxide thickness plays a greater role as compared to temperature and pressure when determining the growth rate of very thin oxide films. Besides, data in Fig. 5 present an upright-parabolic shape for 100 and 200 mbar samples, indicating that the activation energy is gradually increasing with temperature, and in our case, with film thickness. A non-linear relationship among Arrhenius plot data concerning <1100 °C on Si-face oxide films can be observed. It must be noticed that the thickest Si-face oxide film in this temperature range is ∼4 nm (see Fig. 2), value that is similar to the maximum thickness of the interfacial layer, as observed in Fig. 3. We remind that oxidation time, temperature, and pressure can influence the amount of incorporated oxygen in the film that is estimated as film thickness, depending on the mechanism that is taking place. In these very early steps of oxygen incorporation, mechanisms other than the reaction of Si atoms with oxygen appear to play a role as will be elucidated and discussed in the following.

The reduction in the oxidation rate and increasing E_a found for Si-face oxide films could be related to atom emission from the interface, because, according to Kouda *et al.*,[26] the reduction in the atom emission process, which reduces the initial oxidation rate, occurs until the interfacial region reaches its maximum width. By verifying 900 °C and 1000 °C Si-face film characteristics in Fig. 3, one can note that this is the interval in which the oxide film starts to reach SiO_2 stoichiometry, meaning that the interfacial region has reached its maximum development. This situation is analogous to that

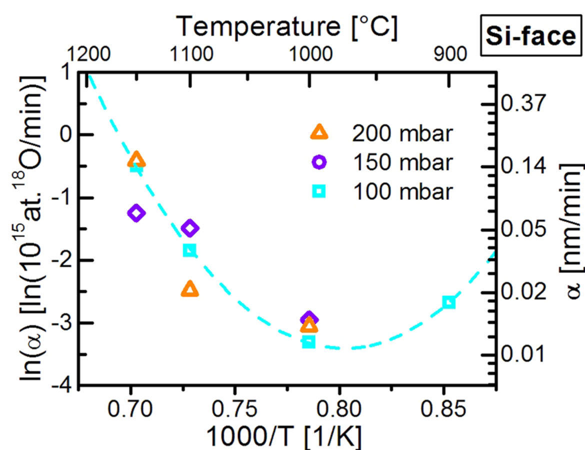

FIG. 5. Arrhenius plots for (0001) Si-face samples. Used $^{18}O_2$ pressures are indicated. Activation energies (E_a) could not be numerically determined because data points presented a non-linear relationship. The dashed parabola is only to guide the eyes. The overall experimental inaccuracy of 10% is about the size of the points. Growth rates are the slopes of the straight lines concerning Si-face data of different sets of samples (oxidized for various times) presented in Fig. 2.

described by Kouda *et al*. Taking the Arrhenius equation into account, a reduction in the oxidation rate can be associated with an increasing E_a, due to varying oxidation mechanisms. Thus, we can infer that the increasing E_a found for Si-face oxide films may be associated with the step-by-step accumulation of the emitted atoms leading to a gradual variation of the oxidation mechanism. From Fig. 5, we observe that E_a keeps varying until the case of films grown at 1100 °C whose thickness is ∼4 nm, as seen in Fig. 2, suggesting that accumulation of emitted atoms is not yet saturated at this thickness.

Moreover, if we consider that atom emission from the substrate is ruling oxide growth at this stage, the very high initial growth rate could also be related to the "active oxidation mode,"[27] where oxide growth occurs in the oxide surface rather than in the interface.[8] Figure 4 reveals that the influence of oxygen pressure is negligible in the oxygen incorporation of very thin films, suggesting that there is enough oxygen to react with emitted atoms even at the lowest pressure tested. This behavior is similar to what was observed in other works,[26] corroborating that the limiting step of the oxidation seems not to be related to the availability of the oxidant species, being limited by atom emission and active oxidation in the interfacial region[10] for films thinner than 4 nm.

As we have reported before,[23] O incorporation can be expressed as the product of oxygen pressure and oxidation time ($p \times t$) for ^{18}O areal densities between 10^{16} and 1.1×10^{17} atoms/cm^2. Figure 6 presents ^{18}O incorporation as a function of ($p \times t$) for samples of this work. One can see that linear relationships are observed in all datasets, except those indicated in Fig. 6(b). These data points, concerning Si-face samples oxidized at 900 and 1000 °C, are not considered to be linear since the adjusted R-square coefficient is rather low. This indicates that the linear ($p \times t$) relation is not valid for films thinner than ∼4 nm grown on the Si-face, corresponding to when the interfacial region is still being formed. Again, it could be an evidence that atom emission from the substrate and active oxidation are ruling oxide growth in this stage.

It can be seen in Fig. 7 that linear Arrhenius relationships were observed for C-face oxide films in all pressures investigated. However, for a given pressure, two different slopes, represented by solid and dashed lines, were found. This indicates that not all data obtained using a given $^{18}O_2$ pressure participate in the same linear behavior, suggesting that there is a change in the oxidation mechanism in all sets of samples. Such changes are indicated by solid and dashed fittings. Knowing that different slopes represent different activation energies and that the oxide growth rate is thickness-dependent,[10,28] we track back to Fig. 2 and observe that the change in the oxidation mechanism occurs when the oxide film is around 10 nm. This means that the activation energy calculated for 200 mbar samples (1.8 eV) was obtained from oxide growth rates of films that are in the most part thicker than ∼10 nm, while for 100 mbar samples, 1.2 eV activation energy was originated by films that are in the most part thinner than ∼10 nm. This suggests that one oxidation mechanism takes place for oxides thicker than ∼10 nm and a different oxidation mechanism rules oxide growth of films thinner than ∼10 nm. This is corroborated by Fig. 8, where it is shown that some oxide films thicker than ∼10 nm do not follow the same

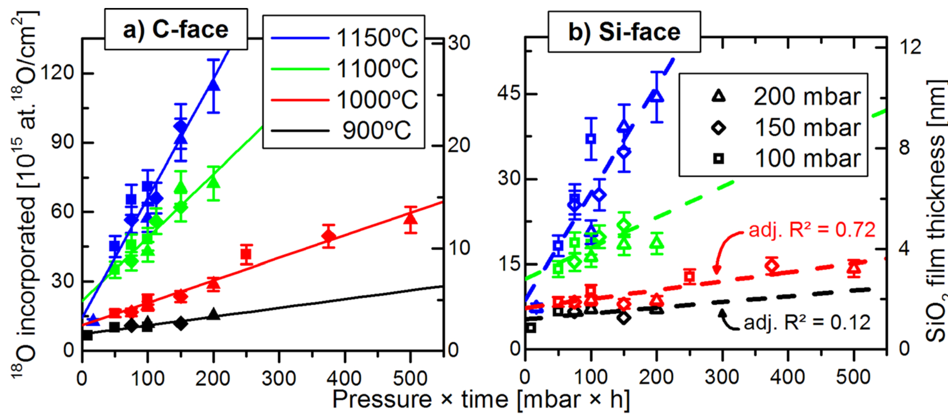

FIG. 6. Relationship between the oxygen incorporation and the product of oxidation pressure and oxidation time. Both graphs share the same symbol key and axes units. The adjusted R-square coefficients are shown for (b) Si-face oxides oxidized at 900 and 1000 °C, suggesting that data relationships are not linear. Bars represent an overall experimental inaccuracy of 10%.

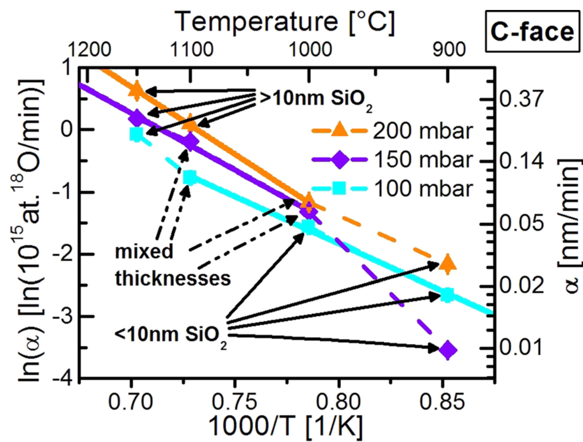

FIG. 7. Arrhenius plots for growth rates of $(000\bar{1})$ C-face samples. Calculated activation energies (E_a) were obtained from the solid lines to be 1.8 eV for 200 mbar samples (orange triangles), 1.5 eV for 150 mbar samples (purple diamonds), and 1.2 eV, for 100 mbar samples (cyan squares). Dashed fittings indicate changes in the oxidation mechanism. Arrows indicate thicknesses of most part of the films used to calculate growth rates. "Mixed thicknesses" correspond to sets of samples that include similar amounts of films with thickness larger and smaller than 10 nm. Bars represent an overall experimental inaccuracy of 10% and are about the size of the points. Growth rates are the slopes of the straight lines concerning C-face data of different sets of samples (oxidized for various times) presented in Fig. 2.

relationship between thickness and oxidation temperature as oxide films thinner than ~10 nm. For 150 mbar samples, growth rates were extracted from sets of samples with comparable amounts of films thicker than 10 nm and thinner than 10 nm, yielding an activation energy of 1.5 eV, which is in between the other two activation energies obtained. Data in Fig. 8(a) show us that samples oxidized for 60 min presented a higher ^{18}O incorporation when submitted to higher pressures. However, this cannot be stated for 30 min samples [Fig. 8(b)], case that is similar to the one observed for Si-face oxide films, corroborating the idea that pressure does not play a great role in the incorporation of oxygen in the early steps of oxidation. The mentioned changes in the oxidation mechanism taking place at different thicknesses can also explain the fact that the oxide growth rate for 100 mbar samples decreases in Si-face oxides when temperature changes from 900 to 1000 °C and increases in C-face oxides in which the incorporation of oxygen is larger.

Massoud's empirical equation,[29] proposed for Si oxidation, was used by Yamamoto *et al.* for describing oxide growth of very thin SiO_2 films on SiC empirically.[30] In their equation, there is a parameter called "characteristic length," which, according to Goto *et al.*, indicates at which oxide thickness the balance of accumulation and consumption of interstitial atoms (i.e., the saturation of emitted atoms) occurs.[28] Values for the characteristic oxide length for C-face can be found in the literature[28,31] and are in agreement with the approximate oxide thickness where the oxidation mechanism change was observed in the present work, which is about 10 nm for the C-face. Moreover, other researchers also observed that oxygen partial pressure has no influence in the characteristic length.[26,30] This also occurred in the present case, where the different $^{18}O_2$ pressures used did not

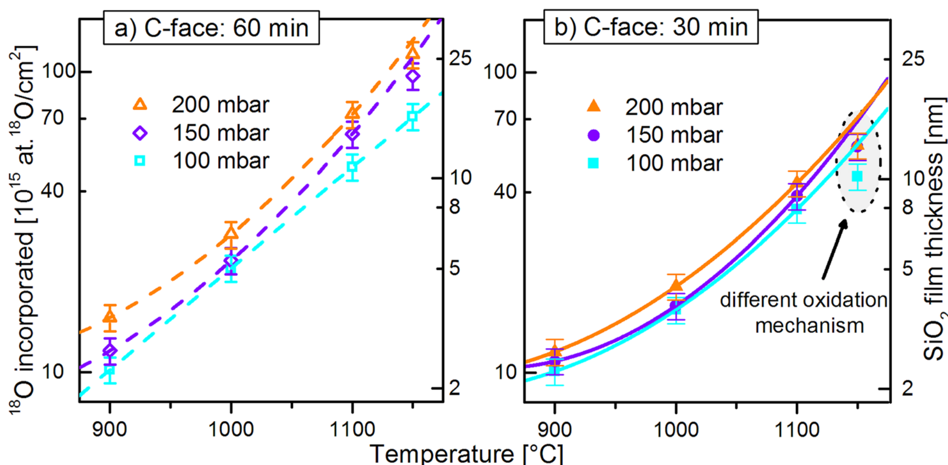

FIG. 8. Temperature dependence of ^{18}O incorporation for C-face oxide films. Points represent experimental data and lines represent fitting curves in (a) for 60 min samples and in (b) for 30 min samples. Fitting curves are only to guide the eyes. Used $^{18}O_2$ pressures are indicated. The ellipse highlights samples whose oxidation mechanism has changed as compared to the one valid for the remaining oxide films. Axes are the same for both (a) and (b). Bars represent an overall experimental inaccuracy of 10%.

induce significant alterations in oxygen incorporation during the growth of the first nanometers of oxide [Fig. 8(b)]. Thus, the oxidation mechanism change observed in the present work for C-face films could be assigned to the saturation of emitted atoms, which occurs when the oxide film thickness is near the characteristic length (~10 nm). Hence, the E_a of 1.2 eV found for the 100 mbar samples (related mostly to <10 nm oxide films) is closely related to interfacial atom emission. On the other hand, since emission saturation is reached in ~10 nm oxide films, $E_a = 1.8$ eV found for 200 mbar samples (related mostly to >10 nm oxide films) concerns mainly the SiC oxidation reaction. We believe that the intermediary value found for 150 mbar samples ($E_a = 1.5$ eV) represents a situation where both interfacial atom emission and SiC reaction with oxygen processes are occurring simultaneously in comparable amounts, evidencing a non-abrupt transition between the interfacial atom emission ruled process and the SiC oxidation reaction ruled process.

IV. CONCLUSIONS

In summary, we showed that different oxidation mechanisms take place in the early steps of SiC dry thermal oxidation and discussed them in terms of strain generated in the interfacial region, atom emission from the substrate, and oxidation reactions as the oxide film becomes thicker. We observed a very rapid growth in Si-face oxide films in their primary stage, which was associated with the active oxidation mode that seems to take place until the oxide film reaches the thickness corresponding to the maximum width found for the interfacial layer, namely, 4 nm. The linear ($p \times t$) relation with thickness appears to be invalid for oxide films in this first growth regime. We showed that this interfacial region between SiC and the oxide film consists of silicon oxycarbides and that it may be generated due to the accumulation of interstitial atoms in a gradual process. In the case of oxide films thicker than ~4 nm, our results suggest that there may be a strong correlation between C and Si emission from the substrate and the limiting step for oxide films with thicknesses below the characteristic length, which appears to be about 10 nm for the present C-face oxide films. On the other hand, for C-face oxide films thicker than the characteristic length, the oxidation reaction seems to act as the limiting step. The activation energies of those processes were determined as 1.2 and 1.8 eV, respectively. In addition, we observed that pressure exerts minimal or no influence in the growth of the first nanometers of the oxide film on both faces.

ACKNOWLEDGMENTS

The authors would like to acknowledge Laboratório de Implantação Iônica UFRGS for the nuclear reactions, INCTs Namitec and Ines, MCT/CNPq, CAPES, and FAPERGS for financial support.

[1]P. G. Neudeck, "Silicon carbide technology," in *The VLSI Handbook*, 2nd ed. (CRC/Taylor & Francis, 2007), pp. 5–1/5–34, ISBN: 0-8493-4199-X.
[2]G. G. Jernigan, R. E. Stahlbush, and N. S. Saks, Appl. Phys. Lett. **77**, 1437 (2000).
[3]G. V. Soares, C. Radtke, I. J. R. Baumvol, and F. C. Stedile, Appl. Phys. Lett. **88**, 041901 (2006).
[4]E. Pitthan, R. Palmieri, S. A. Corrêa, G. V. Soares, H. I. Boudinov, and F. C. Stedile, ECS Solid State Lett. **2**(1), P8–P10 (2013).
[5]S. A. Corrêa, C. Radtke, G. V. Soares, I. J. R. Baumvol, C. Krug, and F. C. Stedile, Electrochem. Solid-State Lett. **11**(9), H258–H261 (2008).
[6]C. Radtke, I. J. R. Baumvol, J. Morais, and F. C. Stedile, Appl. Phys. Lett. **78**, 3601 (2001).
[7]Y. Hijikata, H. Yaguchi, and S. Yoshida, Appl. Phys. Express **2**, 021203 (2009).
[8]Y. Hijikata, Y. Akasaka, S. Yagi, and H. Yaguchi, Mater. Sci. Forum **778–780**, 553–556 (2014).
[9]Y. Hijikata, R. Asafuji, R. Konno, Y. Akasaka, and R. Shinoda, AIP Adv. **5**, 067128 (2015).
[10]D. Goto and Y. Hijikata, J. Phys. D: Appl. Phys. **49**, 225103 (2016).
[11]W. Kern, *Handbook of Semiconductor Wafer Cleaning Technology: Science, Technology, and Applications* (Noyes Publications, 1993), ISBN: 0-8155-1331-3.
[12]W. Kern and D. A. Puotinen, RCA Rev. **31**, 187 (1970).
[13]C. Driemeier, L. Miotti, R. P. Pezzi, K. P. Bastos, and I. J. R. Baumvol, Nucl. Instrum. Methods Phys. Res., Sect. B **249**, 278 (2006).
[14]I. J. R. Baumvol, Surf. Sci. Rep. **36**, 1–166 (1999).
[15]E. Pitthan, S. A. Corrêa, G. V. Soares, C. Radtke, and F. C. Stedile, Nucl. Instrum. Methods Phys. Res., Sect. B **332**, 56–59 (2014).
[16]W. M. Haynes, *CRC Handbook of Chemistry and Physics*, 92nd ed. (CRC Press, Boca Raton, FL, 2011), ISBN: 1439855110.
[17]E. Szilágyi, P. Petrik, T. Lohner, A. A. Koós, M. Fried, and G. Battistig, J. Appl. Phys. **104**, 014903 (2008).
[18]I. C. Vickridge, I. Trimaille, J.-J. Ganem, S. Rigo, C. Radtke, I. J. R. Baumvol, and F. C. Stedile, Phys. Rev. Lett. **89**, 256102 (2002).
[19]B. Hornetz, H.-J. Michel, and J. Halbritter, J. Vac. Sci. Technol. A **13**, 767 (1995).
[20]G. G. Jernigan, R. E. Stahlbush, M. K. Das, J. A. Cooper, Jr., and L. A. Lipkin, Appl. Phys. Lett. **74**, 1448 (1999).
[21]F. C. Stedile, C. Radtke, G. V. Soares, E. Pitthan, R. Palmieri, and S. A. Corrêa, Mater. Sci. Forum **717–720**, 747–752 (2012).
[22]E. Pitthan, S. A. Corrêa, G. V. Soares, H. I. Boudinov, and F. C. Stedile, Appl. Phys. Lett. **104**, 111904 (2014).
[23]E. Pitthan, L. D. Lopes, R. Palmieri, S. A. Corrêa, G. V. Soares, H. I. Boudinov, and F. C. Stedile, APL Mater. **1**, 022101 (2013).
[24]X. Li, A. Ermakov, V. Amarasinghe, E. Garfunkel, T. Gustafsson, and L. C. Feldman, Appl. Phys. Lett. **110**, 141604 (2017).
[25]R. H. Kikuchi and K. Kita, Appl. Phys. Lett. **104**, 052106 (2014).
[26]K. Kouda, Y. Hijikata, S. Yagi, H. Yaguchi, and S. Yoshida, J. Appl. Phys. **112**, 024502 (2012).
[27]N. S. Jacobson and D. L. Myers, Oxid. Met. **75**, 1–25 (2011).
[28]D. Goto, Y. Hijikata, S. Yagi, and H. Yaguchi, J. Appl. Phys. **117**, 095306 (2015).
[29]H. Z. Massoud, J. D. Plummer, and E. A. Irene, J. Electrochem. Soc. **132**, 2685 (1985).
[30]T. Yamamoto, Y. Hijikata, H. Yaguchi, and S. Yoshida, Jpn. J. Appl. Phys., Part 1 **47**(10), 7803–7806 (2008).
[31]V. Šimonka, A. Hössinger, J. Weinbub, and S. Selberherr, J. Appl. Phys. **120**, 135705 (2016).